


 Cite this: *RSC Adv.*, 2020, 10, 18512

Raman spectroscopy-*in situ* characterization of reversibly intercalated oxygen vacancies in α -MoO₃†

 Isaías de Castro Silva, Alice Cosenza Reinaldo, Fernando Aparecido Sigoli  and Italo Odone Mazali *

This work reports on the *in situ* strategy to reversibly generate or suppress oxygen vacancies on α -MoO₃ which were probed by Raman spectroscopy. Reversible changes in two features of the α -MoO₃ Raman spectrum could be correlated to the generation of oxygen vacancies: displacement of the T_b band frequency and the intensity decrease of the symmetrical stretching (ν_s) band. These two features could be used to qualitatively describe oxygen vacancies. Raman results also indicate that oxygen vacancies are located in the interlayer region of the α -MoO₃ lattice. This observation is corroborated by *in situ* X-ray diffraction, which also indicates the absence of nonstoichiometric phase transitions.

 Received 7th February 2020
 Accepted 4th May 2020

DOI: 10.1039/d0ra01207f

rsc.li/rsc-advances

1. Introduction

Molybdenum–oxygen systems include a series of nonstoichiometric solids, in which the oxygen/molybdenum ratio varies between 3 (Mo^{VI}O₃) and 2 (Mo^{IV}O₂).¹ Some values of the oxygen/molybdenum ratio have nonstoichiometric crystalline phases¹ that are well characterized by X-ray diffraction (XRD) and can be classified, according to their crystalline structure as derived from α -MoO₃, ReO₃ or W₁₈O₄₉ structures.¹ Although the changes in the oxygen/molybdenum ratio in these oxides are almost always followed by nonstoichiometric phase transitions,² the presence of oxygen vacancies is an important feature to take into account when molybdenum oxides are applied as catalysts,^{3,4} anode materials for lithium-ion batteries,⁵ gas sensors,^{6,7} electrochromic devices,⁸ and surface-enhanced Raman spectroscopy substrates.⁹

Raman spectroscopy is another tool to characterize nonstoichiometric molybdenum oxides. The α -MoO₃ Raman spectrum is sensitive to particle sizes and the generation of oxygen vacancies.^{3,10} The intensity of the symmetrical stretching (ν_s) band near 820 cm⁻¹ depends on the presence of oxygen vacancies and the intensity ratio of the two bands between 280 and 300 cm⁻¹ can be used to estimate the oxygen/molybdenum ratio in the range from 2.94 to 3.³ However, if the latter bands are convoluted this methodology cannot be applied.

This work reports on the observation of changes in the Raman spectrum of α -MoO₃ submitted to an *in situ* gas–solid reaction

capable of reversibly generate or suppress oxygen vacancies. Nonstoichiometric phase transition was not observed during experiments, as indicated by *in situ* XRD measurements, allowing a qualitative evaluation of oxygen vacancies by Raman spectroscopy.

2. Experimental section

2.1. Synthesis

The synthesis procedure was adapted from a previous report.¹¹ An amount of 7 mL of nitric acid 3 mol L⁻¹ was added to a solution consisting of 0.4900 g of (NH₄)₆Mo₇O₂₄·4H₂O dissolved in 13 mL of deionized water. The final solution was stirred for 5 min, open to the air, before being transferred to a 50 mL poly(tetrafluoroethylene)-lined stainless-steel autoclave. The autoclave was held at 180 °C for 20 h. After cooling, the obtained white solid was filtered and washed several times with ethanol and deionized water and dried at 60 °C for 12 h.

2.2. Characterization

X-ray powder diffraction. These *in situ* analyses were carried out controlling the temperature and atmosphere, at D10B-XRD line of Brazilian Synchrotron Light Laboratory (LNLS), using the Canário furnace and a Mythen linear detector [resolution of 0.005° (2 θ)]. The sample was macerated and slightly pressed-on stainless steel sample holders and the incident radiation wavelength was 1.5498 Å. All diffractograms were collected with the same number of incident photons per detector position, always with the rotation of the sample. The analyses were conducted in the temperature range from 100 to 400 °C with a heating rate of 15 °C min⁻¹ under O₂-containing atmosphere. The gases utilized as atmospheres were: 100% He, 20% O₂/He

Laboratory of Functional Materials– Institute of Chemistry, University of Campinas – UNICAMP, P. O. Box 6154, 13083-970, Campinas, SP, Brazil. E-mail: mazali@unicamp.br

† Electronic supplementary information (ESI) available. See DOI: 10.1039/d0ra01207f



and 5% H₂/He, and the flow rate employed was 100 mL min⁻¹. The sample was exposed to the O₂- or H₂-containing atmospheres alternately (30 minutes of exposure in each one), with a purge of He during 5 minutes between atmosphere changes.^{12–14} Three cycles of atmosphere changes (C_n, where *n* is the number of cycles) were carried out at 400 °C.

Scanning electron microscopy (SEM). The images were obtained in a Quanta FEG 250 microscope operating at 20 kV.

Raman spectroscopy. A Horiba Jobin Yvon T64000 spectrometer, coupled with an Olympus BX41 microscope and charge-coupled device detector, was used in Raman measurements. Incident radiation wavelength was 633 nm from a He–Ne laser (Research Electro-Optics). The spectrometer slit was set at 20 μm, resulting in a spectral resolution of 0.39 cm⁻¹. Spectra were obtained with 2 accumulations of 30 seconds each. The crystalline silicon band at 520.07 cm⁻¹ was used in spectrometer calibration.

A Linkam TS1500 stage, coupled with the Linkam T95-HT controller, was used to *in situ* control temperature (resolution of 1 °C) and atmosphere. In a manner similar to XRD with *in situ* control of temperature and atmosphere, the atmosphere was alternated between 2% H₂/Ar and O₂ at 400 °C (30 min of exposure in each one), always with an N₂ purge flow (5 min) between atmosphere changes. The flow rates were adjusted to 150 mL min⁻¹, and the sample was always heated under O₂, at the rate of 20 °C min⁻¹. A total number of three cycles of atmosphere change was carried out at 400 °C.

Oxygen storage capacity (OSC). The sample was analyzed in a TA Instruments SDT Q600. Approximately 11 mg of MoO₃ samples were placed in an alumina crucible and dried, under the O₂-containing atmosphere at 80 °C until reaching a nearly constant value of mass. After that, the sample was heated to 400 °C at 10 °C min⁻¹ under O₂-containing atmosphere. In a manner similar to XRD with *in situ* control of temperature and atmosphere, the atmosphere was alternated between 2% H₂/Ar and compressed dry air at 400 °C (30 min of exposure in each one), with no purge flow between atmosphere changes. Three cycles of atmosphere change were carried out. The OSC value was calculated considering the final value of mass before each change of atmosphere.

3. Results and discussion

Peaks observed in the diffractogram obtained at room temperature are indexed to the α-MoO₃ orthorhombic phase and β-MoO₃ monoclinic phase (Fig. 1). The diffractogram is dominated by (0*k*0) peaks of the α-MoO₃ phase, where “*k*” stands for an even number, which is a consequence of preferential growth of the crystallites in the [010] direction, or “*b*” axis.^{4,15,16} A complete indexation of the observed peaks at room temperature is found in ESI, Table S1.†

One can see in SEM images that the sample is constituted of needle-like crystals (Fig. 2), with a preferential direction of growth, as pointed out by XRD measurement.

Particle size counting shows that MoO₃ crystals have an average size of 4696 nm in length and 386 nm in width, and the

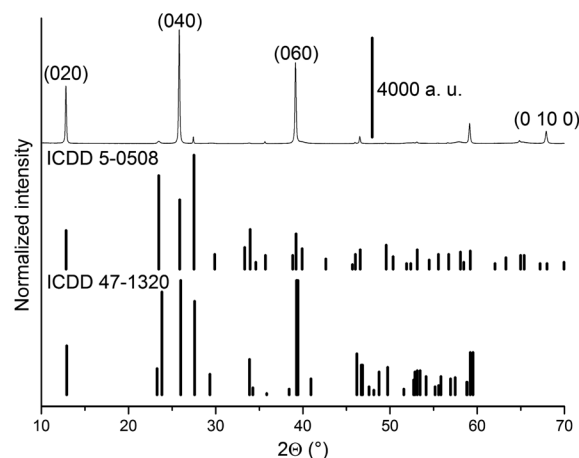


Fig. 1 Diffractogram obtained for MoO₃ sample at 22 °C under 20% O₂/He. The MoO₃ files ICDD 5-0508 (α-MoO₃) and 47-1320 (β-MoO₃) are shown as vertical lines.

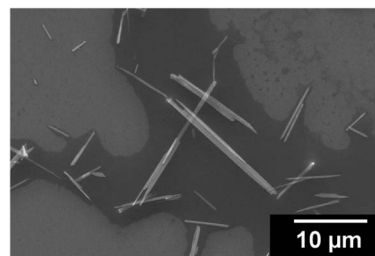


Fig. 2 SEM image of MoO₃ crystals.

mode size range (*ca.* 30%) being 719–5000 nm in length and 250–375 nm in width (Fig. 3).

The observed bands in the Raman spectrum (Fig. 4) are listed in Table 1 and are attributed to the α-MoO₃ orthorhombic phase. This solid can be described as a layered structure composed of linear chains of [MoO₃] unities. If it is considered that the molybdenum ions have a distorted tetrahedral coordination, two oxygen ions are single coordinated to

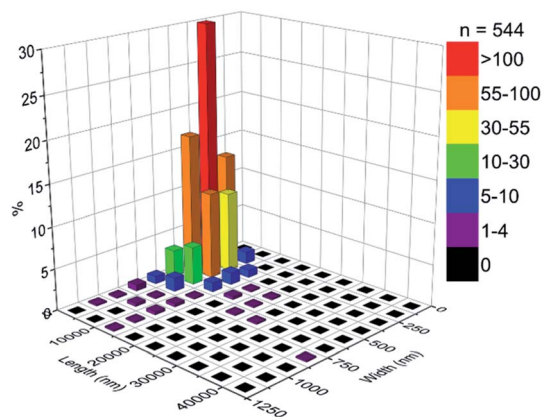


Fig. 3 Particle size distribution of MoO₃ crystals.



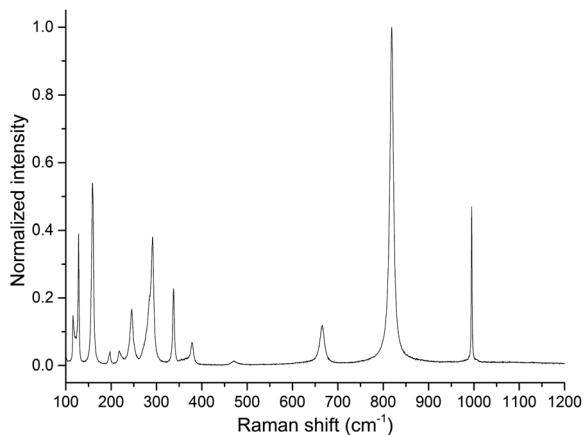


Fig. 4 Raman spectrum of MoO₃ sample obtained at 23 °C under static air inside the heating stage.

Table 1 Attribution of the bands observed in the Raman spectrum of the MoO₃ sample

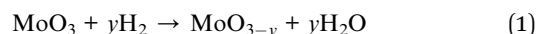
Band frequency (cm ⁻¹)	Representation ¹⁷	Attribution ¹⁷
116	B _{2g}	Translational chain mode along "c" direction (T _c)
128	B _{3g}	Translational chain mode along "c" direction (T _c)
159	A _g /B _{1g}	Translational chain mode along "b" direction (T _b)
197	B _{2g}	τ O=Mo=O
218	A _g	Rotational chain mode along "c" direction (R _c)
246	B _{3g}	τ O=Mo=O
291	B _{3g}	ω O=Mo=O
338	A _g /B _{1g}	δ O-Mo-O
379	B _{1g}	δ O=Mo=O (scissoring)
471	A _g /B _{1g}	ν, δ O-Mo-O
666	B _{2g} /B _{3g}	ν O-Mo-O
819	A _g /B _{1g}	ν _s O=Mo=O
995	A _g	ν _{as} O=Mo=O

a molybdenum ion and are called terminal oxygens (Mo=O). The other one is called bridging oxygen, represented as Mo-O, and is coordinated to two molybdenum ions.¹⁷

The band at 285 cm⁻¹, attributed to a B_{2g} wagging mode of terminal oxygens, is observed as a shoulder of the band at 291 cm⁻¹. The intensity ratio of the bands at 285 and 291 cm⁻¹ may be used to determine the oxygen/molybdenum ratio, in the range from 2.94 to 3.³ However, as one can observe from the Raman spectrum (Fig. 4), the precise determination of intensities ratio requires a comprehensive methodology.

Raman spectra with *in situ* control of temperature and atmosphere are shown in Fig. 5 and 6. A displacement of T_b (A_g/B_{1g}) Raman band to lower frequencies was observed upon heating, a phenomenon attributed to phonon decay,¹⁸ lattice expansion¹⁹ and generation of oxygen vacancies (ESI, Fig. S1†).

As *in situ* Raman results reveal, the exposure to the H₂-containing atmosphere at 400 °C also causes a displacement of the T_b Raman band (Fig. 5). Band maxima wavenumber were obtained from the most intense spectral point. The average displacement, calculated considering the values of T_b band maxima obtained from the 3 spectra in each atmosphere, was 1.09 cm⁻¹, observed between the spectra under H₂ in relation to spectra under O₂ (Fig. 5 b). A displacement to lower frequency values of α-MoO₃ Raman bands is expected if the interaction between the layers of the crystal is weakened, in a manner that the observed Raman band frequencies should resemble more a single layer than the whole crystal.²⁰ This is attributed to the generation of oxygen vacancies and water release,²¹ as shown in eqn (1).



A displacement to lower frequencies of the T_b band was observed when α-MoO₃ was heated to 375 °C under reduced pressure of 10⁻¹ Pa for 10 h.²² Moreover, the generation and suppression of oxygen vacancies is a reversible process at 400 °C, since the T_b Raman band exhibit roughly the same frequency after one cycle of atmosphere change.

The intensity ratio of T_c bands can be used to estimate α-MoO₃ particle sizes.^{3,10} However, in one reference the ratio

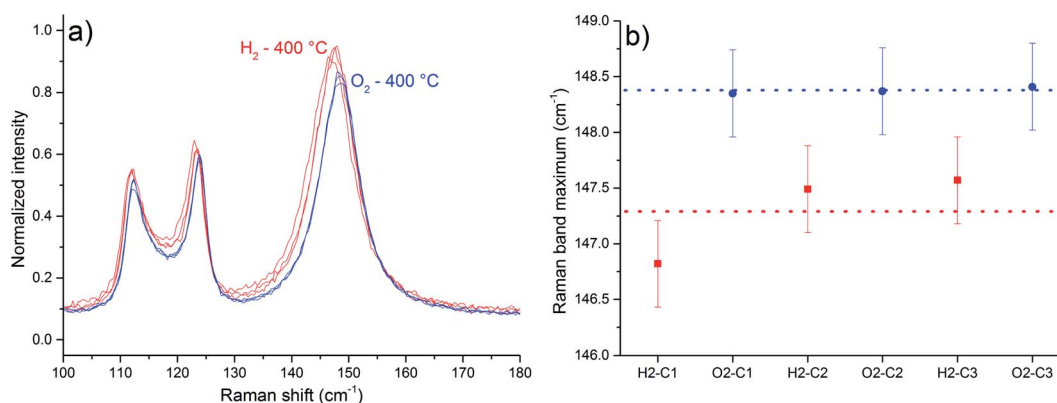


Fig. 5 Part of the Raman spectra obtained at 400 °C for MoO₃ sample, normalized in intensity of ν_s band (a). The average displacement observed for the T_b band under H₂ was 1.09 cm⁻¹ (b). The blue ones were obtained after O₂ exposure, and the red ones were obtained after H₂ exposure. The bars represent spectral resolution – 0.39 cm⁻¹.



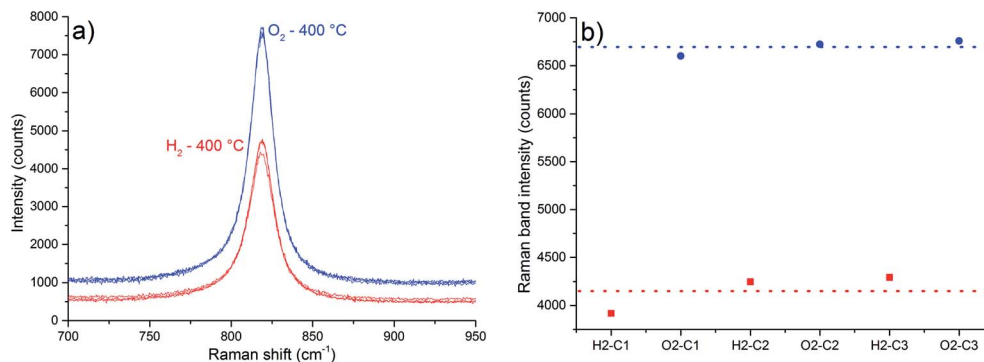


Fig. 6 Part of the Raman spectra obtained at 400 °C for the MoO₃ sample, comprising the ν_s band (a). The average decrease in intensity observed under H₂ was approximately 38% (b). The blue ones were obtained after O₂ exposure, and the red ones were obtained after H₂ exposure.

Table 2 Intensity ratio of T_c modes in α -MoO₃ Raman spectra obtained at 400 °C

	$I_{123}(\text{B}_{3g})/I_{112}(\text{B}_{2g})$		$I_{123}(\text{B}_{3g})/I_{112}(\text{B}_{2g})$
H ₂ -C1	1.225	O ₂ -C1	1.244
H ₂ -C2	1.125	O ₂ -C2	1.178
H ₂ -C3	1.138	O ₂ -C3	1.196

$I(\text{B}_{3g})/I(\text{B}_{2g})$ increases as the size diminishes,¹⁰ and in the other, the ratio $I(\text{B}_{3g})/I(\text{B}_{2g})$ decreases as the particle size diminishes.³ However, just the first reference shows the Raman spectra, therefore we expect the increase in the $I(\text{B}_{3g})/I(\text{B}_{2g})$ ratio as the size diminishes. Based on the latter premise, it is not possible to infer any change in the particle sizes as a function of thermal treatments (Table 2).

The band at 819 cm⁻¹, attributed to the symmetric stretching of the terminal oxygens (ν_s band), is sensitive to oxygen vacancies.³ An intensity increase of this band was observed *in situ* after reacting nonstoichiometric α -MoO₃ with propene and O₂, a consequence of oxygen vacancies suppression.³ One attempt to explain this fact is based on the following aspects:³ when oxygen vacancies are generated, there is also the formation of [Mo⁵⁺O₅] sites. An electronic transition from this site to a normal site of the crystal represented as [Mo⁵⁺O₅]-[Mo⁶⁺O₆] → [Mo⁶⁺O₅]-[Mo⁵⁺O₆], is called intervalence charge transfer (IVCT). According to Dieterle *et al.*,³ the energy of this IVCT transition would be near the energy of the excitation laser (633 nm – 1.96 eV), based on the deconvolution of the diffuse reflectance absorption spectra, and it is supposed to increase in energy as more oxygen vacancies are present in α -MoO₃ lattice.³ Therefore, a resonant Raman-like effect would be observed when oxygen vacancies are generated. Once it is considered the Stokes branch of the Raman scattering, it is possible to occur the reabsorption of the scattered light, affecting the intensity of the Raman spectrum. The most reabsorbed scattered radiation would be the one with energy close to the excitation laser. In other words, it is expected that the bands with lower wavenumbers would present the highest values of intensity decrease. Supposing that the maximum of the IVCT transition varies with

Table 3 Average intensity of Raman bands of α -MoO₃ at 400 °C and their relative decrease in intensity after H₂ exposure

Band frequency at 400 °C (cm ⁻¹)	Average intensity under O ₂ (counts)	Average intensity under H ₂ (counts)	Decrease in intensity (%)
112	3068	2120	30.9
123	3697	2461	33.44
148	5586	3868	30.75
194	592	468	20.9
212	432	389	10
238	1042	782	25.0
285	2973	2035	31.6
335	1461	1000	31.5
374	392	321	18
664	648	414	36.1
819	6695	4152	37.98
992	2784	1722	38.17

stoichiometry, and the incident radiation does not, a specific value of the IVCT transition energy would result in the most intense Raman spectrum, which implies that a specific value of

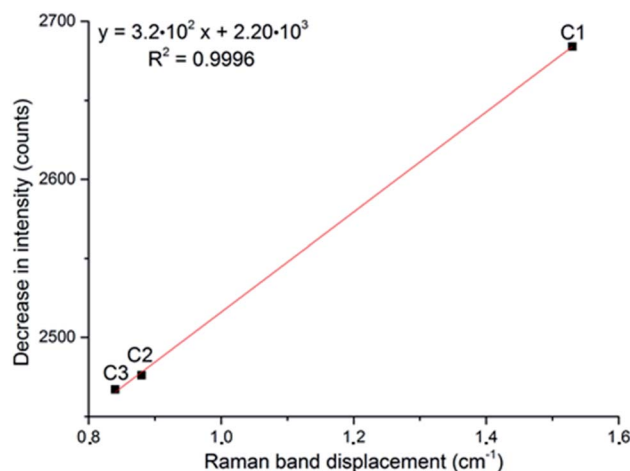


Fig. 7 Correlation of the displacement of the T_b band frequency and the decrease in intensity of the ν_s band, at 819 cm⁻¹, after exposure to H₂ during three cycles (C#).



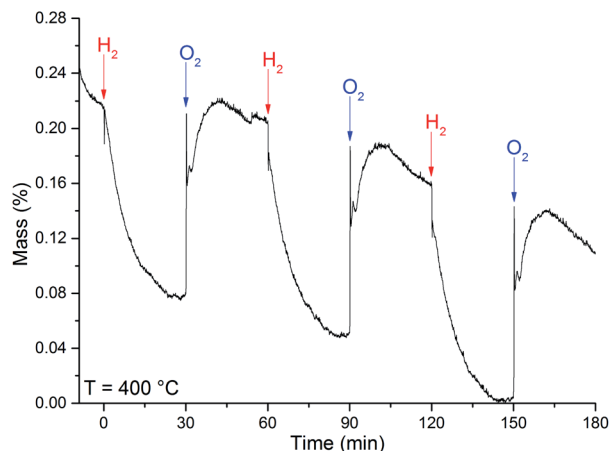


Fig. 8 OSC curve obtained at the temperature of 400 °C for the MoO₃ sample. The arrows indicate when the referred gas was introduced in the system.

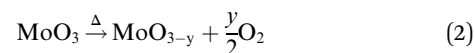
nonstoichiometric degree of the α -MoO₃ would result in the most intense Raman spectrum.

However, the described proposal³ is based on the intensity of the ν_s band observed in different samples, with different particle sizes. The size of the particles may affect the intensity of the Raman spectrum.^{23–34} Yet, according Dieterle *et al.*,³ the energy value of the IVCT transition is calculated based on the deconvolution of the diffuse reflectance absorption spectrum, rather than

a clearer spectral feature. In our case Raman spectra were obtained *in situ*, so the spectra are obtained from the same sample point. As the results in Table 2 suggest, there is no change in particle size during experiments. The highest values of intensity decrease were observed for the bands more distant in energy to the excitation radiation (Table 3), which is contrary to the described proposal.³ In addition, Mestl *et al.*,¹⁰ have found that the intensity decrease of Raman bands is independent of the excitation energy in the range from 458 nm to 622 nm.¹⁰

If the displacement of the T_b Raman band is plotted against the decrease in intensity of the ν_s band, a linear relationship is obtained (Fig. 7). This fact suggests that both these observations are related to the same effect, the generation of oxygen vacancies in α -MoO₃, and could be considered to evaluate its oxygen vacancies. Contrary to the previous report³ which stated that a determined value of nonstoichiometry may lead to the most intense ν_s band, this correlation suggests that the most intense ν_s band is observed in the sample with the highest oxygen/molybdenum ratio, the stoichiometric α -MoO₃.

It was observed a loss of mass upon heating, due to the formation of oxygen vacancies,²² according to eqn (2).



If it is considered that the starting dried sample was composed of stoichiometric MoO₃, the loss of mass upon heating resulted in a variation of the nonstoichiometric degree

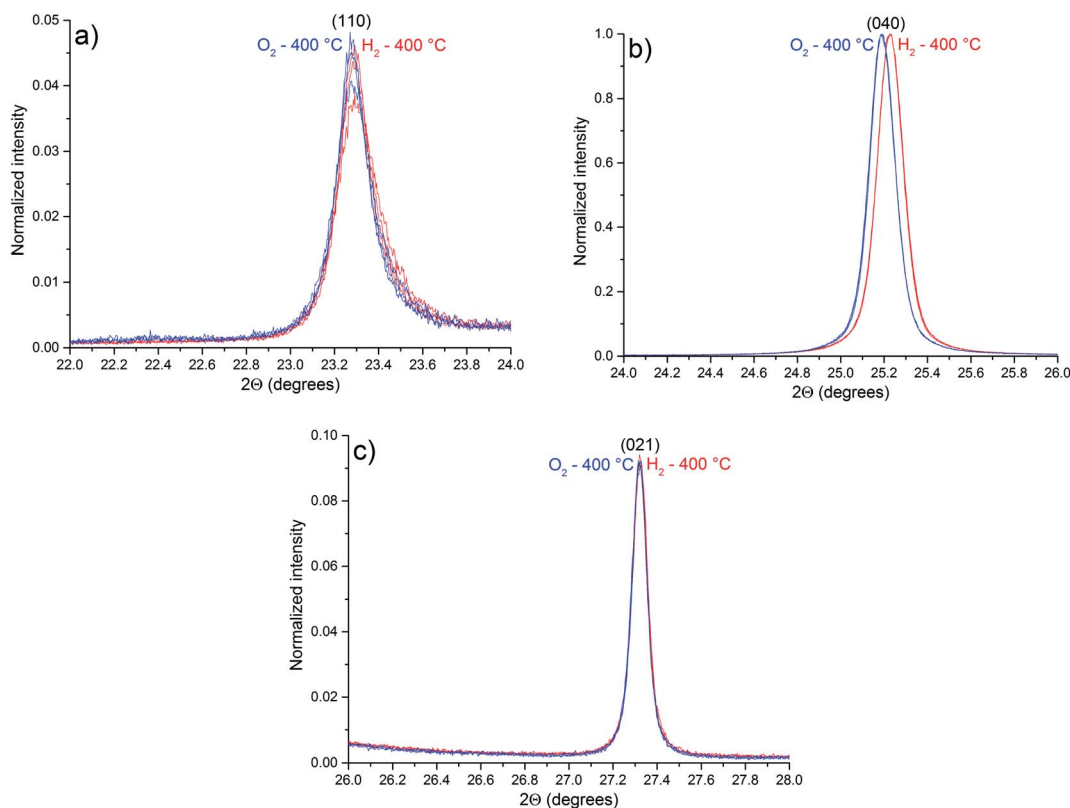


Fig. 9 Parts of the diffractograms of α -MoO₃ planes: (a) (110); (b) (040); and (c) (021), obtained at 400 °C. The blue ones were obtained after O₂ exposure and the red ones were obtained after H₂ exposure.



Table 4 Observed shifts in XRD peaks of α -MoO₃ after exposure to H₂ at 400 °C. The last plane was not observed in the 22 °C diffractogram and could not be indexed

Plane	Average 2θ under H ₂ (°)	Average 2θ under O ₂ (°)	Difference in 2θ (H ₂ -O ₂) (°)
020	12.531	12.515	0.016
040	25.227	25.187	0.040
041	35.225	35.205	0.020
060	38.251	38.198	0.053
210	45.759	45.739	0.020
002	49.531	49.543	-0.012
211	51.815	51.745	0.060
171	57.005	56.955	0.050
081	57.963	57.907	0.056
190	63.793	63.728	0.065
062	64.263	64.244	0.019
0 10 0	66.213	66.141	0.072
*	69.361	69.275	0.086

of 0.039 (MoO_{2.961}). This value of stoichiometry is not compatible with any other crystalline phase of the molybdenum-oxygen system.¹

The calculated OSC value of $35 \pm 3 \mu\text{mol (O}_2\text{) g}^{-1}$, at 400 °C, were obtained from the OSC curve in Fig. 8.

The loss of mass under H₂ exposure is attributed to the formation of water and oxygen vacancies (eqn (1)). These vacancies are suppressed under O₂ exposure. The reincorporation of oxygen ions in the MoO₃ lattice is accompanied by a gain of mass. Due to the adsorption of gases, it is not possible to obtain any quantitative measurement of the nonstoichiometric degree. However, if we consider that the difference in mass is solely due to generation and suppression of oxygen vacancies, the variation of the nonstoichiometric degree, achieved after H₂ exposure at 400 °C, can be estimated to be 0.010 ± 0.002 (MoO_{2.951}). This value of stoichiometry is not compatible with any other crystalline phase of the molybdenum-oxygen system.¹

Part of the diffractograms with *in situ* control of temperature and atmosphere, illustrating the peaks (110), (040) and (021) of the α -MoO₃ phase, are shown in Fig. 9.

Compared to the diffractogram of Fig. 1, the diffraction peaks observed in Fig. 9 are shifted to minor values of 2θ due to thermal expansion of the lattice. As pointed out by OSC results, no phase transition was observed during experiments (Fig. S2†). Table 4 lists the observed planes that are shifted after exposure to H₂ at 400 °C (Fig. S3†).

Some diffraction peaks of the α -MoO₃ phase are shifted to higher values of 2θ after H₂ exposure due to a lattice contraction after exposure to H₂, a consequence of the oxygen vacancies generation. The reason for the α -MoO₃ (0*k*0) peaks shift to higher values of 2θ (Table 4), in “*b*” direction, is the location of the oxygen vacancies in the interlayer region, as pointed out by *in situ* Raman results. The terminal oxygens in the interlayer region have the lowest calculated energy value of oxygen vacancy formation.^{35,36} However, the diffraction peak attributed to (002) plane is shifted to lower values of 2θ after H₂ exposure, indicating an expansion of the lattice in the “*c*” direction. These

observations are in contrast with a previous report,³ when an expansion in the “*b*” direction and a contraction in the “*c*” direction were reported, suggesting that oxygen vacancies tend to replace bridging oxygens. However, the results here obtained indicate that oxygen vacancies tend to accumulate in the interlayer region, replacing terminal oxygens, leading to the decrease in the layer distance, and a contraction in “*b*” direction. As a consequence, Raman bands are shifted to lower frequencies, resembling more the calculated spectrum of a single layer than the spectrum of the crystal.²¹

4. Conclusion

After submitting MoO₃ need-like crystals to an *in situ* strategy to reversibly generate or suppress oxygen vacancies, it was possible to observe reversible changes in two α -MoO₃ Raman features: the displacement of T_b band and the decrease in intensity of the ν_s band. The displacement of the T_b band is attributed to the weakening of α -MoO₃ layers interaction, probably due to the location of oxygen vacancies in the interlayer region. XRD results corroborate the location of oxygen vacancies in the interlayer region, as the small value of vacancy formation energy is observed in this region. The decrease in intensity of the ν_s band was not possible to be attributed, but the proposal of a resonant Raman-like effect was contested. Based on that, Raman spectroscopy can provide two distinct manners to qualitative probe oxygen vacancies in α -MoO₃. No non-stoichiometric phase transition was observed by XRD or OSC results, indicating that the observations were, in fact, derived from the generation of oxygen vacancies in the α -MoO₃ structure.

Conflicts of interest

There are no conflicts to declare.

Acknowledgements

The authors gratefully acknowledge CNPq and FAPESP for the financial support. Contributions from Brazilian Synchrotron Light Laboratory (LNLS/CNPEM, Brazil - Proposal 20171016) and Multiuser Laboratory of Advanced Optical Spectroscopy (LMEOA/IQ-UNICAMP) for XRD and Raman measurements, respectively, are also gratefully acknowledged. This is a contribution of the National Institute of Science and Technology in Complex Functional Materials (CNPq-MCT/FAPESP).

References

- 1 L. Kihlberg, in *Nonstoichiometric compounds*, ed. R. Ward, American Chemical Society, 1963, pp. 37–45.
- 2 P. L. Gai, *Philos. Mag. A*, 1981, **43**, 841–855.
- 3 M. Dieterle, G. Weinberg and G. Mestl, *Phys. Chem. Chem. Phys.*, 2002, **4**, 812–821.
- 4 J. González, J. A. Wang, L. Chen, M. Manríquez, J. Salmones, R. Limas and U. Arellano, *J. Solid State Chem.*, 2018, **263**, 100–114.



- 5 D. Wu, R. Shen, R. Yang, W. Ji, M. Jiang, W. Ding and L. Peng, *Sci. Rep.*, 2017, **7**, 44697.
- 6 M. M. Y. A. Alsaif, M. R. Field, B. J. Murdoch, T. Daeneke, K. Latham, A. F. Chrimes, A. S. Zoolfakar, S. P. Russo, J. Z. Ou and K. Kalantar-zadeh, *Nanoscale*, 2014, **6**, 12780–12791.
- 7 N. Illyaskutty, S. Sreedhar, G. S. Kumar, H. Kohler, M. Schwotzer, C. Natzeck and V. P. M. Pillai, *Nanoscale*, 2014, **6**, 13882–13894.
- 8 B. Dasgupta, Y. Ren, L. M. Wong, L. Kong, E. S. Tok, W. K. Chim and S. Y. Chiam, *J. Phys. Chem. C*, 2015, **119**, 10592–10601.
- 9 H. Wu, H. Wang and G. Li, *Analyst*, 2017, **142**, 326–335.
- 10 G. Mestl, T. K. K. Srinivasan and H. Knözinger, *Langmuir*, 1995, **11**, 3795–3804.
- 11 Y. Chen, C. Lu, L. Xu, Y. Ma, W. Hou and J.-J. Zhu, *CrystEngComm*, 2010, **12**, 3740–3747.
- 12 L. Ilieva, P. Petrova, G. Pantaleo, R. Zanella, L. F. Liotta, V. Georgiev, S. Boghosian, Z. Kaszkur, J. W. Sobczak, W. Lisowski, A. M. Venezia and T. Tabakova, *Appl. Catal., B*, 2016, **188**, 154–168.
- 13 C. Andriopoulou, A. Trimpalis, K. C. Petallidou, A. Sgoura, A. M. Efstathiou and S. Boghosian, *J. Phys. Chem. C*, 2017, **121**, 7931–7943.
- 14 I. C. Silva, F. A. Sigoli and I. O. Mazali, *J. Phys. Chem. C*, 2017, **121**, 12928–12935.
- 15 W. Thöni, P. Gai and P. B. Hirsch, *J. Less-Common Met.*, 1977, **54**, 263–271.
- 16 M. Epifani, P. Imperatori, L. Mirengi, M. Schioppa and P. Siciliano, *Chem. Mater.*, 2004, **16**, 5495–5501.
- 17 M. A. Py, P. E. Schmid and J. T. Vallin, *Nuovo Cimento B*, 1977, **38**, 271–279.
- 18 M. Balkanski, R. F. Wallis and E. Haro, *Phys. Rev. B: Condens. Matter Mater. Phys.*, 1983, **28**, 1928–1934.
- 19 J. E. Spanier, R. D. Robinson, F. Zhang, S.-W. Chan and I. P. Herman, *Phys. Rev. B: Condens. Matter Mater. Phys.*, 2001, **64**, 245407.
- 20 M. A. Py and K. Maschke, *Physica B*, 1981, **105**, 370–374.
- 21 W. E. Garner, *J. Chem. Soc.*, 1947, 1239–1244.
- 22 G. Mestl, P. Ruiz, B. Delmon and H. Knözinger, *J. Phys. Chem.*, 1994, **98**, 11269–11275.
- 23 M. V. Pellow-Jarman, P. J. Hendra and R. J. Lehnert, *Vib. Spectrosc.*, 1996, **12**, 257–261.
- 24 H. Wang, C. K. Mann and T. J. Vickers, *Appl. Spectrosc.*, 2002, **56**, 1538–1544.
- 25 C. H. Chio, S. K. Sharma, P. G. Lucey and D. W. Muenow, *Appl. Spectrosc.*, 2003, **57**, 774–783.
- 26 Y. Hu, H. Wikström, S. R. Byrn and L. S. Taylor, *Appl. Spectrosc.*, 2006, **60**, 977–984.
- 27 Z.-P. Chen, L.-M. Li, J.-W. Ji, A. Nordon, D. Littlejohn, J. Yang, J. Zhang and R.-Q. Yu, *Anal. Chem.*, 2012, **84**, 4088–4094.
- 28 N. Townshend, A. Nordon, D. Littlejohn, J. Andrews and P. Dallin, *Anal. Chem.*, 2012, **84**, 4665–4670.
- 29 P. Allan, L. J. Bellamy, A. Nordon, D. Littlejohn, J. Andrews and P. Dallin, *J. Pharmaceut. Biomed. Anal.*, 2013, **76**, 28–35.
- 30 F. Foucher, G. Lopez-Reyes, N. Bost, F. Rull-Perez, P. Rüßmann and F. Westall, *J. Raman Spectrosc.*, 2013, **44**, 916–925.
- 31 A. Sparén, M. Hartman, M. Fransson, J. Johansson and O. Svensson, *Appl. Spectrosc.*, 2015, **69**, 580–589.
- 32 P. Kristova, L. J. Hopkinson and K. J. Rutt, *J. Phys. Chem. A*, 2015, **119**, 4891–4897.
- 33 P. K. Duy, S. Chun and H. Chung, *Anal. Chem.*, 2017, **89**, 11937–11943.
- 34 D. A. Gómez, J. Coello and S. Maspoch, *Vib. Spectrosc.*, 2019, **100**, 48–56.
- 35 R. Coquet and D. J. Willock, *Phys. Chem. Chem. Phys.*, 2005, **7**, 3819–3828.
- 36 K. Inzani, M. Nematollahi, F. Vullum-Bruer, T. Grande, T. W. Reenaas and S. M. Selbach, *Phys. Chem. Chem. Phys.*, 2017, **19**, 9232–9245.

